International Journal of Naval Architecture and Ocean Engineering 13 (2021) 650–658

Contents lists available at ScienceDirect

International Journal of Naval Architecture and Ocean Engineering

journal homepage: http://www.journals.elsevier.com/international-journal-of-naval-architecture-and-ocean-engineering/

Structural configurations and dynamic performances of flexible riser with distributed buoyancy modules based on FEM simulations

Weimin Chen [a, b, c, *], Shuangxi Guo [b, c], Yilun Li [d], Yuxin Gai [e], Yijun Shen [a, f, **]

[a] State Key Laboratory of Marine Resource Utilization in South China Sea (Hainan University), Haikou, China
[b] Institute of Mechanics, Chinese Academy of Sciences, Beijing, China
[c] School of Engineering Science, University of Chinese Academy of Sciences, Beijing, China
[d] Université Paris-Saclay, CentraleSupélec, CNRS, Laboratoire de Mécanique des Sols, Structures et Matériaux (MSSMat-UMR8579), Gif-sur-Yvette, France
[e] School of Aeronautics Sciences and Engineering, Beihang University, Beijing, China
[f] College of Civil Engineering and Architecture, Hainan University, Haikou, China

ARTICLE INFO

Article history:
Received 25 January 2021
Received in revised form
19 April 2021
Accepted 16 July 2021
Available online 19 July 2021

Keywords:
Deep-sea mining
Flexible riser
Riser configuration
Response and performance

ABSTRACT

Flexible risers are usually used as conveying systems to bring ocean resources from sea bed up to onshore. Under ocean environments, risers need to bear complex loads and it is crucial to comprehensively examine riser's configurations and to analyze structural dynamic performances under excitation of bottom vehicle motions, to guarantee structural safe operation and required service lives.

In this study, considering a saddle-shaped riser, the influences of some important design parameters, including installation position of buoyancy modules, buoyancy ratio and motion of mining vehicle, on riser's configuration and response are carefully examined. Through our FEM simulations, the spatial distributions of structural tensions and curvatures along of riser length, under different configurations, are compared. Then, the impacts of mining vehicle motion on riser dynamic response are discussed, and structural tolerance performance is assessed. The results show that modules installation position and buoyancy ratio have significant impacts on riser configurations. And, an appropriate riser configuration is obtained through comprehensive analysis on the modules positions and buoyancy ratios. Under this proposed configuration, the structural tension and curvature could moderately change with buoyancy modules and bottom-end conditions, in other words, the proposed saddle-shaped riser has a good tolerance performance to various load excitations.

1. Introduction

With the development of offshore oil and gas production and mining industry, riser systems of various configurations have been used for oil/gas/brine/mineral transportation, and they are becoming an important part of the whole production system owing to their complicated configurations and higher economic cost. These riser systems usually be categorized into Top Tension Riser (TTR), Steel Catenary Riser (SCR) and hybrid riser (Lou et al., 2019). Among these risers, with the increase of water depth, upper-end tension of SCR increases profoundly, which limits its further application in deep waters (Wang and Duan, 2015). And, TTR may suffer from a large tension due to motion of top-end float under environmental loads, while hybrid riser's joint is one of the difficult problems to deal with. Therefore, alternative riser configurations have been continually proposed to meet the requirements for deep water production, such as compliant vertical access risers and steel lazy-wave riser (Santillan and Virgin, 2011; Pearce et al., 1988; Tian et al., 2015) for oil/gas platform, or saddle-shaped riser (Wang et al., 2007) for ocean mining systems.

To ensure structural safety and effective operation along with a sufficient service life of riser system, riser configuration needs to be designed carefully based on comprehensive examination of its structural response, such as the tension, stress and displacement of a riser under excitations of environmental loads and moving boundary conditions. There have been fruitful researches on responses of popular risers such as TTR, SCR and lazy wave risers. Yin

* Corresponding author.
** Corresponding author. State Key Laboratory of Marine Resource Utilization in South China Sea (Hainan University), Haikou, China.
E-mail addresses: wmchen@imech.ac.cn (W. Chen), yshen2000@163.com (Y. Shen).

Peer review under responsibility of The Society of Naval Architects of Korea.

https://doi.org/10.1016/j.ijnaoe.2021.07.003

et al. (2019) studied the dynamic responses of a TTR caused by vessel motion using experimental tests and numerical simulations. Cheng et al. (2020) presents a time-domain numerical scheme to study the dynamic performance of the lazy wave riser subjected to the vessel offsets and wave-current loads, and the influences of buoyancy segment length on the riser's dynamic behavior are studied. Chatjigeorgiou, (2010a, b) presented the nonlinear dynamic behavior of a submerged, extensible catenary riser conveying fluid and subjected to top imposed excitations, the results showed that only the out-of-plane response is affected by the internal flow. Chatjigeorgiou (2010a, b) investigated the effect of the steady flow inside the pipe on both the in-plane and the out-of-plane vibrations through his numerical simulations. Guo et al. (2018) studied the influences of the amplitude/frequency of the top vessel motion, along with the buoyancy modules distribution along structural length, on dynamic responses of lazy-wave and hybrid-tower types of risers. Jang and Kim (2019) studied VIV(vortex-induced vibration) response of a long flexible lazy-wave riser using CFD simulations and Li et al. (2018) studied the multi-frequency vortex-induced vibration of a TTR in lineally sheared fluid field using the numerical approach.

These researches mainly focus on the riser responses caused by boundary motion and environment loads, there is relatively little research on configuration analysis of risers. Mao et al. (2016) established an analysis model of the actual riser string configuration to study the mechanical behavior of a drilling riser. It was found that riser configuration has a significant effect on riser mechanical behavior, and, particularly, on structural bending moment by affecting distribution of bending stiffness, tension on cross section and ocean environments. Kim and O'Reilly (2019) investigated the dynamics and stability of a catenary type flexible riser, and he presented the way that the internal fluid being conveyed destabilizing certain static configurations. Ai et al. (2019) studied the stress and fatigue damage along the lazy-wave risers with different distribution of buoyancy modules using genetic algorithms. However, as for saddle-shaped riser, there have been few reports on structural response. As we know, saddle-shaped riser, with distributed buoyancy modules along its length needs to bear complex loads such as structural gravity, buoyancy forces, wave and current forces. Therefore the assessments of its structural safety and reliability become quite challenging. Moreover, for case of deep-sea mining operation, the moving boundary conditions, coming from top-end float and/or bottom end mining vehicle motions, would bring an additional concern to riser deformation and dynamic responses. To guarantee safe operation and required service life of these risers, it is crucial to comprehensively and carefully examine riser's configurations and to analyze structural dynamic performances under boundary excitations.

In this study, the overall configuration and dynamic performance of a saddle-shaped riser are studied through carrying out our finite element simulations. Firstly, by examining the structural tension distribution, vertical displacement and curvature, the riser configurations, with different installation position of buoyancy modules and the buoyancy ratio, are comprehensively analyzed. Further, to assess the dynamic performance of the riser, the structural responses under actions of moving mining vehicle are examined, in terms of structural tension, stress level and curvature. And, the locations of those key areas with higher stress and larger curvature are particularly concerned. The results show that the installation position of buoyancy modules could significantly change riser configuration. And the buoyancy ratio of the two buoyancy modules could also effectively reduce the maximum tension and the top tension of the riser. An appropriate riser configuration is obtained through comprehensive design of the modules installation position and buoyancy ratio. It is found that this saddle-shaped riser has a good tolerance performance to the bottom-end excitation.

Here, this study focuses on the global/static response and dynamic performance caused by mining vehicle motion of saddle-shaped riser. And the strength and safety of the risers are investigated through stress and curvature analysis in both static and dynamic cases. As for other riser responses and issues, such as VIV, wave/current forces along with fatigue performance, are beyond the scope of this study.

2. Model descriptions of flexible riser with distributing buoyancies

2.1. Flexible riser with two buoyancy sections

The values of flexible riser parameters here are considered according to the prototype of the Project of the Deep-Ocean Mining System at 1000 m water depth in the South China Sea, and the main structural parameters [6] are listed in Table 1. The top-end of the flexible riser is connected with a lifting pipe at 900 m water depth, and its bottom-end is connected with the mining vehicle at 1000 m water depth. Two sections of buoyancy modules, i.e. buoyancy B and buoyancy C, are installed on the riser, and the riser is shaped like a saddle configuration, shown in Fig. 1. Under the initial condition, the horizontal distance between the top-end, point A, and the bottom-end, point D, is 200 m.

To archive a good mechanical performance during mining operation, riser configuration should be designed carefully. Essentially, riser configuration mainly depends on the values of the parameters of buoyancy modules, e.g. the uplift force, the distribution length, and the installation position of the modules. And the structural tension and stress level are assessed to evaluate the riser performance. The distribution length and position of the buoyancy modules directly affect the stress and tension of riser. On the other hand, the impacts of moving boundaries, coming from top-end float oscillation and/or bottom-end vehicle motion, on riser performances should be considered so as to avoid excessive curvature or axial compression along riser length.

Here, the overall configuration and dynamic performance of a saddle-shaped riser are studied through carrying out our finite element simulations. The responses, including the structural overall configurations, riser tensions and curvatures under different load cases, are calculated and compared, while the installation positions of buoyancy modules along with the mining vehicle position change in different cases. The distribution length of Buoyancy B and C is 20 m. L_B indicates the position of Buoyancy B, and F_B is the equivalent buoyancy force. L_C and F_C respectively represent the buoyancy position and force of Buoyancy C. The buoyancy ratio is defined as F_B/F_C. The overall riser length, ranging from the upper-end A to the bottom-end D, is 400 m.

The cases with different values of buoyancy locations and buoyancy forces (buoyancy ratio) are summarized in Table 2. It is seen that through Cases 1–4, the influences of the installation position of buoyancy modules on riser configurations, tensions and

Table 1
Parameters of the flexible riser.

Parameter	Value
Outside diameter	205.0 mm
Inner diameter	150.0 mm
Length	400 m
Weight in water	30.0 kg/m
Tensile stiffness	1.536e9N
Bending stiffness	2.096e4N m^2

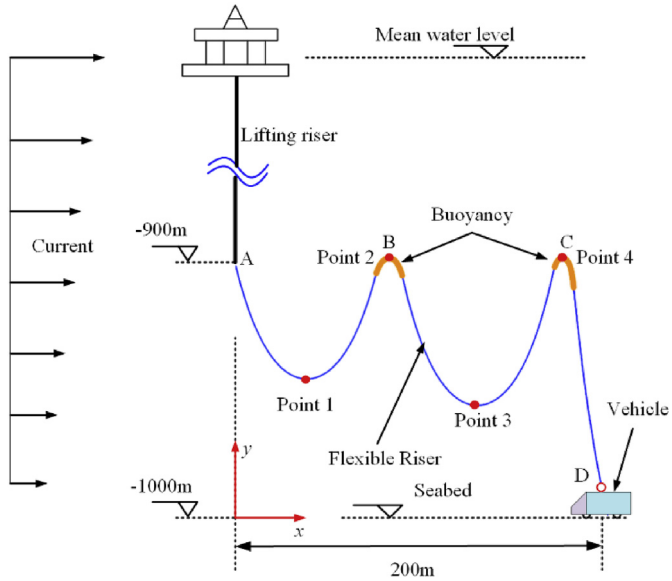

Fig. 1. Schematic of the saddle-shaped flexible riser.

curvatures can be studied. And, through Case 4–6, the influences of the buoyancy ratio on the riser performance during operation situations can be presented.

2.2. FE models

The Finite Element (FE) simulation (Zienkiewicz and Taylor, 2005) is used in this study to calculate riser response under different loading cases. The whole riser is divided into a set of beam elements, and the beam nodes are arranged at each installation position of the buoyancy modules as shown in Fig. 2. We assume that the motion of the riser is in the *x*-*y* plane (see Fig. 1), so only the in plane displacements are considered for each beam element. The displacement vector of the beam element is

$$U_e = [u_i \quad v_i \quad \theta_i \quad u_{i+1} \quad v_{i+1} \quad \theta_{i+1}]^T \tag{1}$$

where u and v are the axial and translational displacements respectively. θ is the rotational angle, and i is the node number of the beam element. For simplicity, the displacement vector is divided into two parts, i.e. the axial part and the lateral part

$$\begin{aligned} U_e^1 &= [u_i \quad u_{i+1}]^T \\ U_e^2 &= [v_i \quad \theta_i \quad v_{i+1} \quad \theta_{i+1}]^T \end{aligned} \tag{2}$$

The shape functions of beam displacement are

Table 2
Location of buoyancy and buoyancy force in different cases.

Cases	L_B	F_B	L_C	F_C
1	123 m–143 m	4.0t	256 m–276 m	8.0t
2	123 m–143 m	4.0t	266 m–286 m	8.0t
3	123 m–143 m	4.0t	276 m–296 m	8.0t
4	123 m–143 m	4.0t	286 m–306 m	8.0t
5	123 m–143 m	4.5t	286 m–306 m	7.5t
6	123 m–143 m	5.0t	286 m–306 m	7.0t

$$\begin{aligned} \mathbf{N}_1(x_e) &= [1 - x_e/l_e, x_e/l_e] \\ \mathbf{N}_2(x_e) &= \left[1 - 3\xi^2 + 2\xi^3, l_e\left(\xi - 2\xi^2 + \xi^3\right), 3\xi^2 - 2\xi^3, l_e\left(\xi^3 - \xi^2\right)\right] \end{aligned} \tag{3}$$

where $\xi = x_e/l_e$ and x_e is the axial location. The strain matrix can be written as

$$B_i(x_e) = \frac{d(N_i)}{d(x_e)} \tag{4}$$

where A_e is the cross area. Then the mass and stiffness matrices of the element can be written as

$$\begin{aligned} K_e^1 &= \int_0^{l_e}\int_{A_e} B_1^T E_e B_1 dA_e dx_e \quad M_e^1 = \int_0^{l_e}\int_{A_e} B_1^T \rho A_e B_1 dA_e dx_e \\ K_e^2 &= \int_0^{l_e}\int_{A_e} B_2^T E_e B_2 dA_e dx_e \quad M_e^2 = \int_0^{l_e}\int_{A_e} B_2^T \rho A_e B_2 dA_e dx_e \end{aligned} \tag{5}$$

where ρ is the density of the riser. As for the beam elements connected with buoyancy modules, the mass of modules should be added to the corresponding mass matrix

$$\begin{aligned} M_e^1 &= \int_0^{l_e}\int_{A_e} B_1^T \rho A_e B_1 dA_e dx_e + M_0 \cdot diag\begin{bmatrix} \delta_i & \delta_{i+1} \end{bmatrix} \\ M_e^2 &= \int_0^{l_e}\int_{A_e} B_2^T \rho A_e B_2 dA_e dx_e + M_0 \cdot diag\begin{bmatrix} \delta_i & 0 & \delta_{i+1} & 0 \end{bmatrix} \end{aligned}$$

where M_0 is the mass of each buoyancy module, and δ_i is a Dirac function and its value is 1 if the node contains a buoyancy module, or 0 otherwise. Assembling the element matrices, we can obtain the mass matrix M_e and stiffness matrix K_e of beam element, and, subsequently, the whole structural matrices. Then the dynamic governing equation, in terms of FE expression, of the flexible riser is

$$[M] \cdot \left[\ddot{U}\right] + [C] \cdot \left[\dot{U}\right] + [K] \cdot [U] = [P] \tag{6}$$

where $[M]$, $[C]$ and $[K]$ are the mass matrix, damping matrix and stiffness matrix respectively. $[U]$ and $[P]$ are the displacement vector and load vector of the whole riser respectively. The damping matrix takes the form of linear superposition of the mass matrix and stiffness matrix. Due to the movement of bottom mining vehicle, the riser may experience a relative motion to the surrounding fluid caused by the movement of the. Therefore, the riser is subjected to fluid forces under mining operation, i.e. the hydrodynamic damping force. The Morison equation is used in this study to calculate the hydrodynamic loads acting on the riser.

$$f = \frac{1}{2}C_d\rho_1 D|\mathbf{V} - \dot{\mathbf{u}}|(\mathbf{V} - \dot{\mathbf{u}}) + C_A\frac{\pi D^2}{4}\rho_1\left(\dot{\mathbf{V}} - \ddot{\mathbf{u}}\right) + \frac{\pi D^2}{4}\rho_1\dot{\mathbf{V}} \tag{7}$$

where D and $\mathbf{V}$ are the structural diameter and the vector of the external fluid velocity, ρ_1 is the density of the fluid, C_d and C_A are the drag coefficient and added mass coefficient.

To solve Eq. (6), the Newmark scheme is used to integrate in time. Assuming the current time step is step n, an estimate of the acceleration at the end of step n+1 will satisfy the following equation of motion:

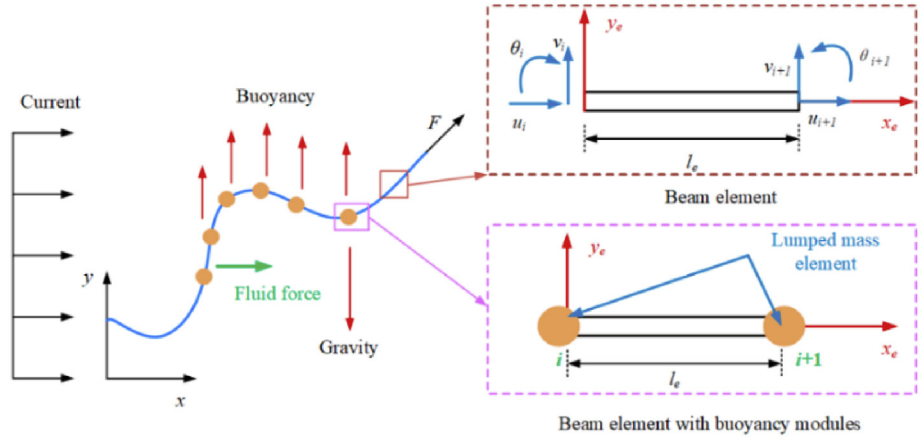

Fig. 2. Beam elements in the local coordinate system.

$$[M]\cdot[a_{n+1}]+[C]\cdot[v_{n+1}]+[K]\cdot[d_{n+1}]=[p_{n+1}] \tag{8}$$

where $[p_{n+1}]$, $[a_{n+1}]$, $[v_{n+1}]$, $[d_{n+1}]$ are the vectors of externally applied loads, estimated acceleration, estimated velocity and estimated displacement at step $n+1$ respectively. The estimates of displacement and velocity are given by:

$$\begin{aligned}[d_{n+1}]&=[d_n]+[v_n]\Delta t+\frac{(1-2\beta)[a_n]\Delta t^2}{2}+\beta[a_{n+1}]\Delta t^2\\ [v_{n+1}]&=[v_n]+(1-\gamma)[a_n]\Delta t+\gamma[a_{n+1}]\Delta t\end{aligned} \tag{9}$$

where is Δt the time step, β and γ are constants, and the values of β and γ are respectively 1/6 and 1/2 in this study.

The expression (9) can be written as:

$$\begin{aligned}[d_{n+1}]&=[D_n]+\beta[a_{n+1}]\Delta t^2\\ [v_{n+1}]&=[V_n]+\gamma[a_{n+1}]\Delta t\end{aligned} \tag{10}$$

The terms $[D_n]$ and $[V_n]$ are predictive and are based on values already calculated. Substituting Eq. (10) in Eq. (8) results in

Then the acceleration $[a_{n+1}]$ can be obtained using Eq. (11), and thus the displacement and velocity vectors in step $n+1$.**1.3 Verifications of the FE Model**

To verify the FEM model, the configuration and tension of a catenary mooring-line is calculated and compared with the experimental results. The parameters of the catenary are listed in Table 3 (José et al., 2017), and Fig. 3(a) shows a schematic diagram of the catenary.

Firstly, two catenary configurations with different horizontal projection, i.e. 19.872 m for Configuration 1 and 19.364 m for Configuration 2, are calculated and compared with the experimental profiles. The comparison of catenary configurations is shown in Fig. 3(b).

To verify the dynamic calculation of the presented model, the displacement responses at different positions along catenary length, with the top-end surge period 3.16s and amplitude 0.125 m, are also compared for case of Configuration 1. In Fig. 4, the numerical and experimental trajectories at the three markers, i.e. located at 1.155 m (Marker 1), 2.149 m (Marker 2), 2.646 m (Marker 3) respectively from the top-end, are presented. It can be seen that both the displacement responses and configurations agree well with the experimental results.

Table 3
Parameters of the catenary mooring-line.

Parameter	Value
Total length	21.0 m
Initial vertical projection	5.0 m
Axial stiffness	3.4e5N
Equivalent hydrodynamic diameter	0.0034 m
Mass per unit length	0.069 kg/m
Wet weight per unit length	0.5872 N/m

3. Numerical results and discussions

Structural safety and operation performance of mining riser, in practice, are directly related to the level of riser tension/stress during mining operation, so it is important to design riser configuration carefully to ensure its safety and reliability. A reasonable arrangement of buoyancy modules and proper buoyancy ratio is a crucial concern during configuration design. On the other hand, the motion of the bottom mining vehicle could also cause changes of structural configuration and tension/stress. In this Section, the riser responses, caused by different installation positions of buoyancy modules, buoyancy ratios and mining vehicle motions, are analyzed. During our calculations, it is assumed that both ends of the riser are hinged supports, and the riser motion is in the *x-y* plane.

$$[M]\cdot[a_{n+1}]+[C]\cdot\{[V_n]+\gamma[a_{n+1}]\Delta t\}+[K]\cdot\left\{[D_n]+\beta[a_{n+1}]\Delta t^2\right\}=[p_{n+1}] \tag{11}$$

3.1. Influences of buoyancy module position on riser performance

To analyze the influences of the installation position of buoyancy modules on riser's responses, we calculated the

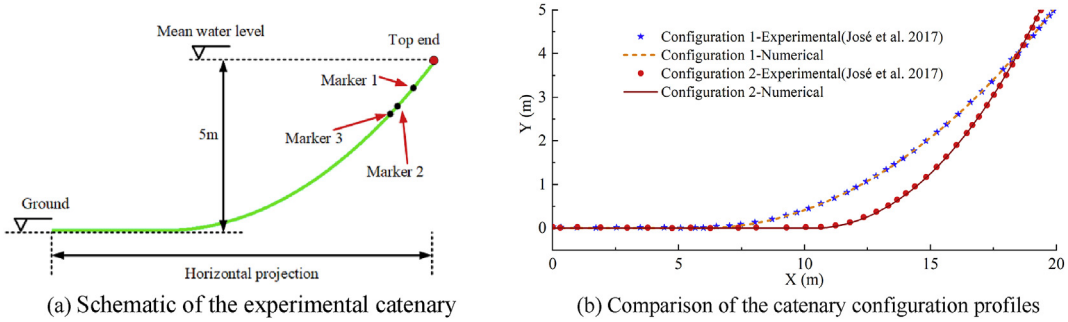

(a) Schematic of the experimental catenary (b) Comparison of the catenary configuration profiles

Fig. 3. Comparison of numerical results with the experimental ones.

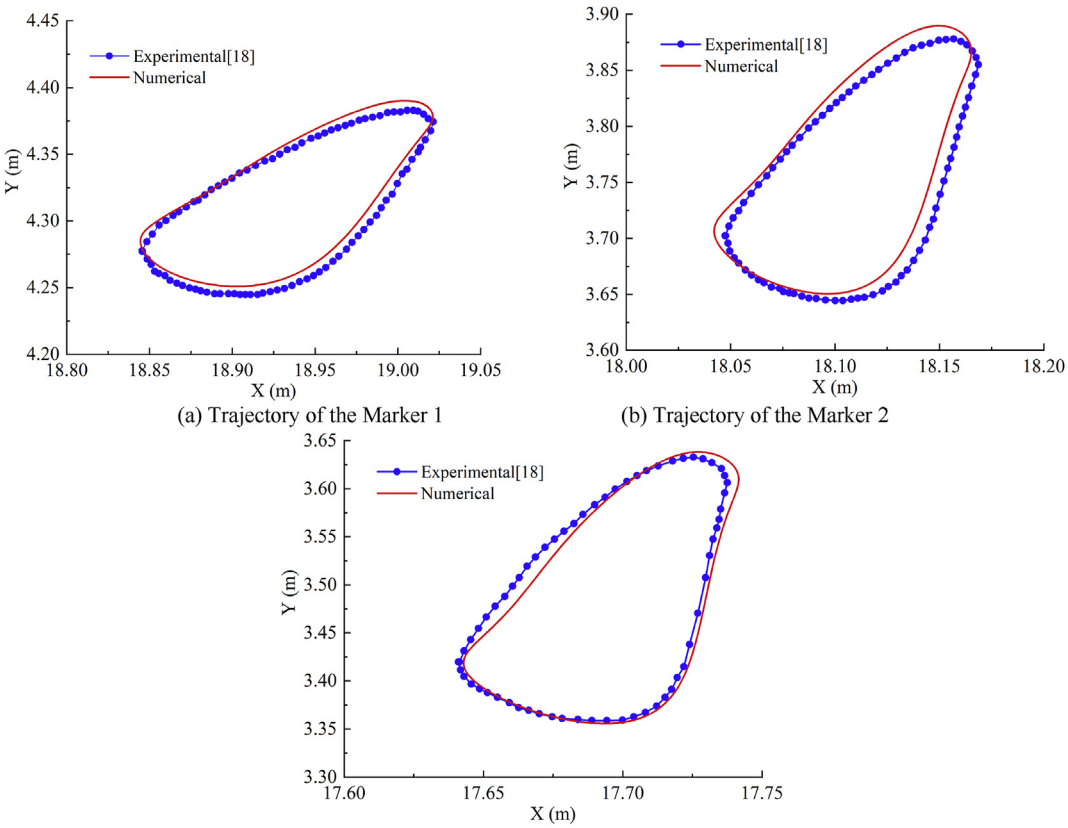

(a) Trajectory of the Marker 1 (b) Trajectory of the Marker 2

(c) Trajectory of the Marker 3

Fig. 4. Comparisons of the numerical and experimental results, in term of the trajectories at the three makers, shown in Fig. 3(a), along the catenary length.

configurations, tensions and curvatures for Cases 1–4, where the position of Buoyancy C moves toward the bottom end of the riser.

The comparisons of riser configurations and tension distributions are shown in Fig. 5. From Fig. 5(a), it can be seen that the position of buoyancy modules has a significant influence on riser configuration. As the position of Buoyancy C moves down toward the riser bottom-end, the overall vertical displacement of the riser gradually drops. Compared with Case 1, the installation position of Buoyancy C is 30 m closer to the bottom end in Case 4, and the vertical height of riser drops up to 40 m. This is because that more buoyancy force provided by Buoyancy C is balanced by the increasing pretension at Point D (in Fig. 1), as Buoyancy C moves toward the bottom-end. Thus leading to a decrease of the riser vertical height so that the upper point (Point A) can provide more load to balance the gravity of riser.

The tension distributions along riser length for different load cases are compared in Fig. 5(b). It can be seen that with the moving of the buoyancy C down toward the bottom-end, the maximum tension tends to decreases, by about 9%, while the tensions at riser's two ends are increased. It is worthwhile to point out that the tension value of the bottom-end should be designed to be less than a certain value, or it should not exceed the value of the gravity of the bottom mining vehicle.

The distributions of the curvatures for the four cases are shown in Fig. 6. We note that the buoyancy installation position has little effect on the maximum curvature, and the reason might be that the maximum curvature mainly depends on the distribution length of the buoyancy modules, which, in all four cases, has the same value, i.e. 0.32/m. It can be seen that, due to the change of buoyancy installation position, the maximum tension decreases by 9%, which may benefit structural safety. But with the moving of Buoyancy C down toward the bottom-end, the overall vertical height of the

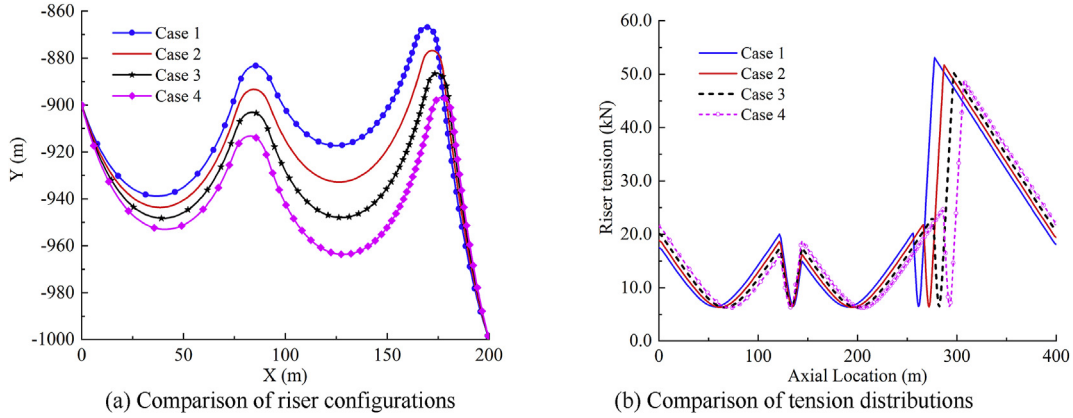

(a) Comparison of riser configurations (b) Comparison of tension distributions

Fig. 5. Influence of buoyancy position on riser's tension and configurations.

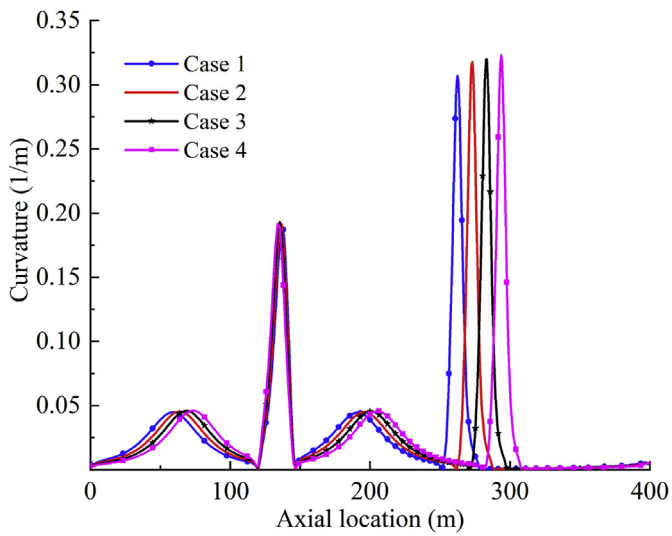

Fig. 6. Influence of buoyancy position on structural curvatures.

riser drops about 40 m, this could raise a risk of riser touching down to seabed. To improve riser configuration, the design of the buoyancy ratio of the two buoyancy sections will be discussed in next section.

3.2. Influences of buoyancy ratio on riser performance

Buoyancy ratio of the two buoyancy sections is also one of important factors that affect riser configuration and responses. Here the influences of buoyancy ratio on riser configuration, tension and curvature are examined, while the position and total buoyancy force remain the same. The riser configurations under different buoyancy ratios, i.e. 0.5 in Case 4, 0.6 in Case 5 and 0.714 in Case 6, are plotted in Fig. 7. It can be seen that buoyancy ratio has a significant impact on the overall configuration. As the buoyancy ratios F_B/F_C increases from 0.5 to 0.714, i.e. F_B increases from 4.0t to 5.0t, the vertical height of the riser at the position of Buoyancy B gets about 40 m larger. Since the bottom-end is always kept in a tensional state, the change of buoyancy can only affect the pretension. This can be further proven in the tension plots presented in Fig. 7(b). The tension distributions along riser length, with different buoyancy ratios, are shown in Fig. 8(a). The maximum tension and the tension at both top-end and bottom-end decrease with the increasing buoyancy ratio. As F_B increases from 4.0t to 5.0t, the maximum tension decreases by about 10%, i.e. from 48.36 KN to 43.47 KN, and the tension at the upper-end drops from 21.49 KN to 16.78 KN, by about 22%. That is mainly because the decrease of F_C could reduce the pretension at the bottom-end, while the increase of F_B could make a larger buoyancy force so as to balance much structural gravity. That could introduce a smaller value of gravity which needs to be balanced by the top tension, in other words the top tension gets smaller.

Fig. 7(c) shows the distributions of the curvatures along the riser length for the three load cases. It is noted that the buoyancy ratio has little effect on the maximum curvatures (around 0.32/m), which actually depends on the distribution length of the buoyancy modules. From the above discussion, we can conclude that Case 5 is the best buoyancy approach, in terms of installation position and equivalent buoyance force ratio of the modules. In this case, the riser tension is relatively smaller and the riser height from the seabed is higher enough (larger than 50 m).

3.3. Dynamic performance under mining vehicle motion

Generally, for risers used for oil conveying whose bottom-end is usually fixed to the seabed well, the boundary conditions can be regarded as fixed conditions. However, for case of deep sea mining, the mining vehicle, connected to the bottom-end of riser, actually moves around during mining operations. That is to say there is an excitation to the riser coming from a moving bottom boundary. In this section, the dynamic response of the riser with the selected configuration (Case 5), caused by the mining vehicle motion, is investigated. And, the riser tension and curvature at key positions are analyzed to evaluate the riser dynamic performance.

In fact, the motion of mining vehicle will directly change the bottom-end position of riser, that is to say the horizontal projection of riser may change. As the length and vertical projection of a riser remain the same, the variation of the horizontal projection will cause a change of its configuration. And consequently, riser's curvature and the angles at top and bottom ends become different, that lead to the changes of axial tension and stress. Therefore, the motion of mining vehicle should be considered comprehensively during riser operation design.

3.3.1. Riser Trajectory & configuration

The dynamic response of the riser under mining vehicle motion, with 200s period and 25 m amplitude, is calculated. The configurations, with different vehicle positions, are shown in Fig. 8, it can be seen that the vehicle motion can significantly change the riser configuration.

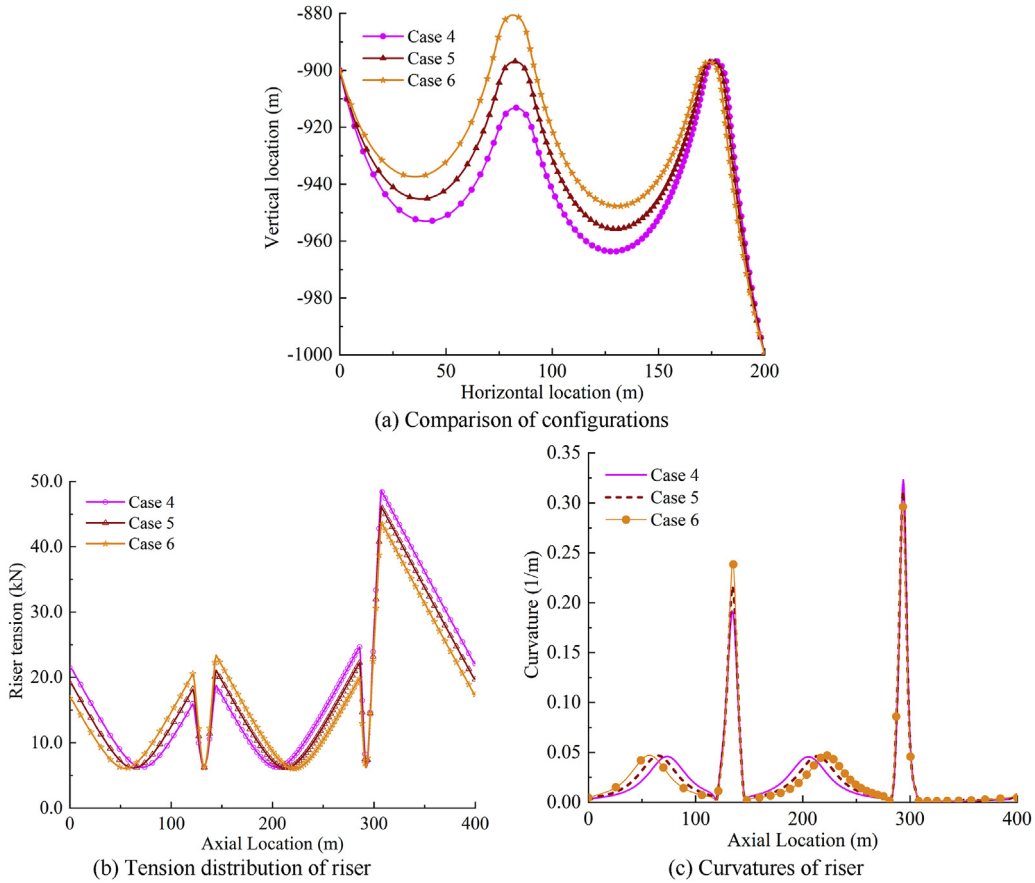

Fig. 7. Riser responses under different buoyancy ratios.

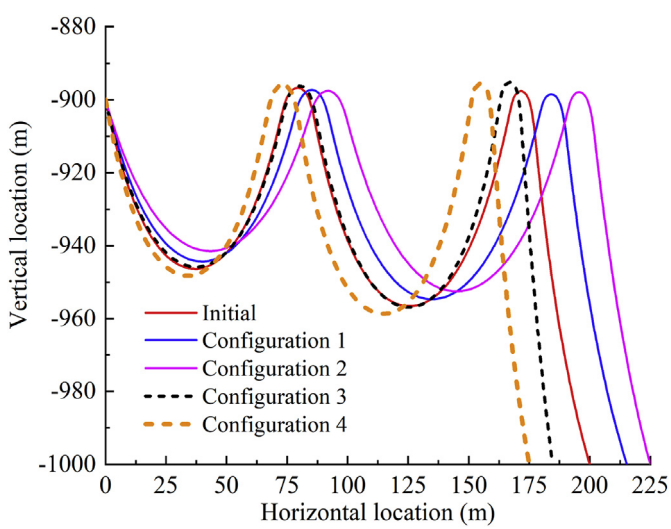

Fig. 8. Riser configurations with different vehicle positions.

And, the displacements of four selected points (Fig. 1) are compared in Fig. 9. It can be seen that, the horizontal displacements decrease gradually, from the point at bottom (mining vehicle) to top-end. However, as for the vertical displacement, its change is more complicated. Or, the most obvious change of structural configuration happens at Point 1, near the free-suspending position, and it should be pay more attention because of potential touch down upon sea bed.

3.3.2. *Temporal-spatial evolution of structural tension and stress*

Typical evolution of the riser tension change is shown in Fig. 10(a), under vehicle motion with 25 m amplitude and 200s period. It can be seen that, the tension abruptly change at the position where the static tension is locally minimum, i.e. around point 1–4 as shown in Fig. 1. And, the maximum amplitude of tension change is about 1.9 kN, it already reaches to 30% of the initial tension value (6.2 kN). Since the tension changes around Point 1, -4 (as shown in Fig. 1) are larger, the fatigue problem at these key points should be paid more attention during structural design and strength check. The temporal-spatial evolution of the bending stress change is presented in Fig. 10(b). Different from the tension, the maximum stress change occurs at the center of buoyancy installation position, the maximum change is about 1.7 MPa and is much larger than other positions. The change of bending stress caused by the mining vehicle motion is 12% of the initial value, and this indicates that the stress response at positions where buoyancy modules are installed, should be checked carefully for sake of structural safety.

During the mining vehicle motion, the maximum and minimum bending stress of the riser at the key point, which locates at 292 m along the axial length (as shown in Fig. 10), is presented in Fig. 11. As a comparison, the results of all cases are also plotted, and it can be seen that the stress differences (Fig. 11(b)) caused by the mining vehicle motion are almost the same, i.e. between 3.05 and 3.25 MPa, for the six cases. This indicates that the presented saddle-shaped riser has a good tolerance performance to the bottom-end excitation.

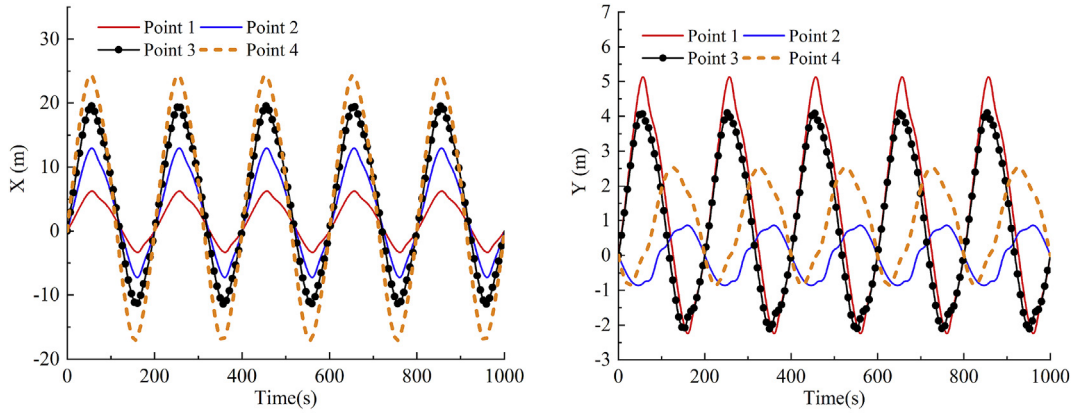

(a) Comparison of the horizontal displacements (b) Comparison of the vertical displacements

Fig. 9. Displacement responses of four selected points along riser length.

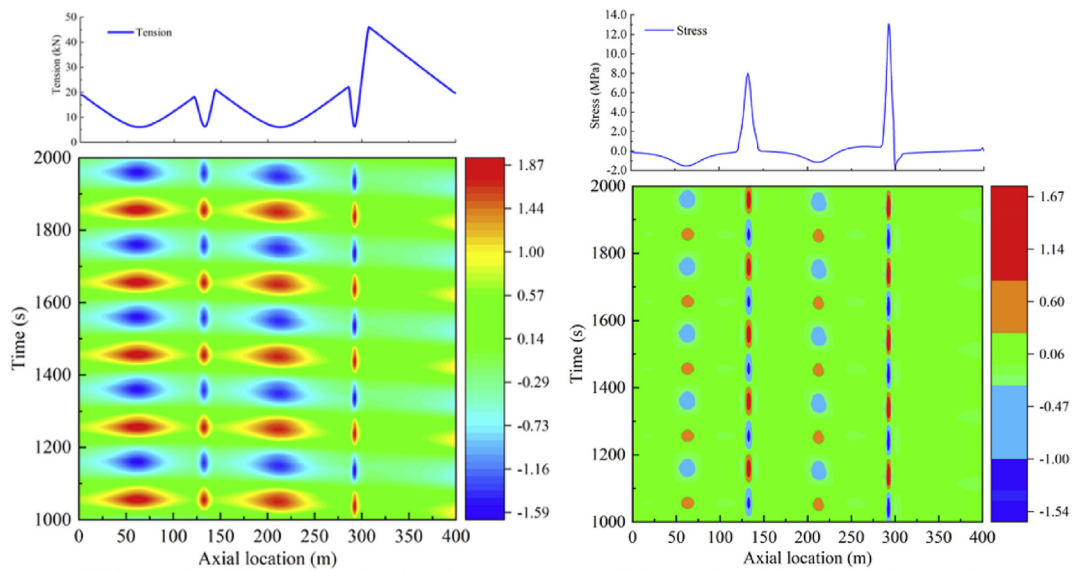

(a) Temporal-spatial evolution of tension change (b) Temporal-spatial evolution of stress change

Fig. 10. Temporal-spatial evolution of tension change and stress change.

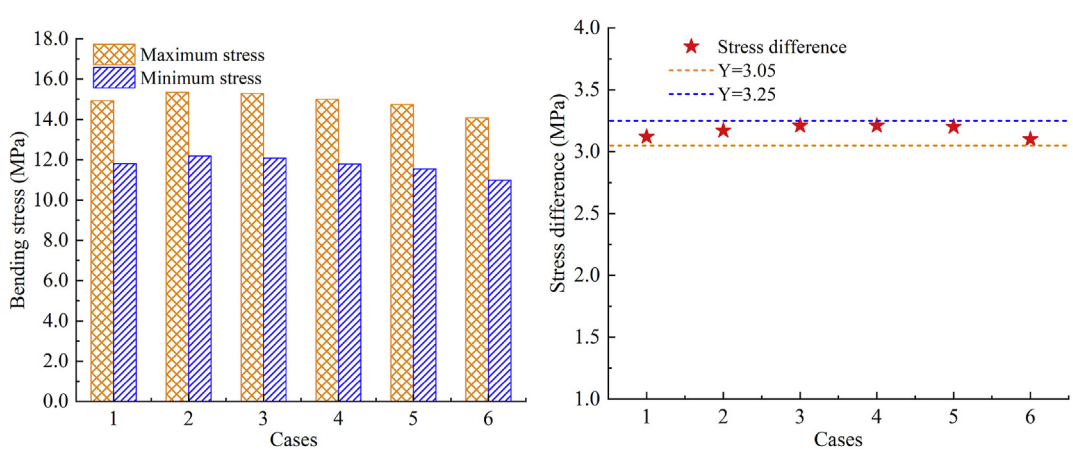

(a) Bending stress of 6 cases (b) Stress differences

Fig. 11. Comparison of bending stress under mining vehicle motion.

4. Conclusions

The response analysis model of saddle-shaped riser is developed based on our finite element simulations. By examining the structural tension, stress and curvature distributions along the riser length, the influences of some important design factors, i.e. the buoyancy position, the buoyancy ratio and the motion of mining vehicle, on riser's configuration and response are examined.

The numerical results show that the buoyancy position and buoyancy ratio have significant impacts on the riser's configuration and tension. For examples, the change of the buoyancy module position could introduce a 46 m decrease of the riser vertical height. And, a small change of the buoyancy ratio can reduce the maximum tension and the top tension respectively by about 10% and up to 22%. Owing to the mining vehicle motion, the maximum tension change occurs at the position where the static tension is locally minimum, and the maximum stress change occurs at the center of buoyancy installation position. These are the hot points that should be pay more attention in structural design. Under this proposed configuration, the structural tension and curvature could moderately change with buoyancy modules and bottom-end conditions, or, in other words, the proposed saddle-shaped riser has a better tolerance performance to the moving vehicle excitation during mining operation.

It should also be pointed out that, in this study, in order to improve the riser's tension level and operational performance, the overall configuration analysis of a saddle-shaped riser is carried out through the FE simulations. Or, our focus is the global/static response and dynamic performance caused by mining vehicle motion of the saddle-shaped riser. More detailed/further work, such as analysis on more detailed local stress, dynamic responses or VIV, along with fatigue performance, would be considered in the future.

Declaration of competing interest

The authors declare there is no conflicts of interest regarding the publication of this paper.

Acknowledgements

The authors of this paper would like to thank the financial supports provided by the research funding sponsored by The State Key Laboratory of Marine Resource Utilization in the South China Sea (Hainan University) (Grant No. MRUKF2021027) and the Strategic Priority Research Programme of the Chinese Academy of Sciences (Grant No. XDA22000000).

References

Ai, S., Xu, Y., Kang, Z., Yan, F., 2019. Performance comparison of stress-objective and fatigue-objective optimisation for steel lazy wave risers[J]. Ships Offshore Struct. 14 (6), 534–544.
Chatjigeorgiou, I.K., 2010a. Three dimensional nonlinear dynamics of submerged, extensible catenary pipes conveying fluid and subjected to end-imposed excitations[J]. Int. J. Non Lin. Mech. 45 (7), 667–680.
Chatjigeorgiou, Ioannis K., 2010b. On the effect of internal flow on vibrating catenary risers in three dimensions[J]. Eng. Struct. 32, 3313–3329.
Cheng, Y., Tang, L., Fan, T., 2020. Dynamic analysis of deepwater steel lazy wave riser with internal flow and seabed interaction using a nonlinear finite element method[J]. Ocean Eng. 209, 107498.
Guo, S.X., Li, Y.L., Li, M., et al., 2018. Dynamic Response Analysis on Flexible Riser with Different Configurations in Deep-Water Based on FEM simulation[C]. OMAE2018. V005T04A016.
Jang, H., Kim, J.W., 2019. Numerical Investigation for Vortex-Induced Vibrations of Steel-Lazy-Wave-Risers: Part II - CFD Study on Long Flexible riser[C]. OMAE 2019. V002T08A031.
José, Azcona, Xabier, et al., 2017. Experimental validation of a dynamic mooring lines code with tension and motion measurements of a submerged chain[J]. Ocean Eng. 129, 415–427.
Kim, H.T., O'Reilly, O.M., 2019. Instability of catenary-type flexible risers conveying fluid in subsea environments[J]. Ocean Eng. 173, 98–115.
Li, Y., Guo, S., Chen, W., 2018. Analysis on multi-frequency vortex-induced vibration and mode competition of flexible deep-ocean riser in sheared fluid fields[J]. J. Petrol. Sci. Eng. 163, 378–386.
Lou, M., Hu, P., Qi, X., et al., 2019. Stability analysis of deepwater compliant vertical access riser about parametric excitation[J]. Int. J. Naval Arch. Ocean Eng. 11, 970–979.
Mao, L., Liu, Q., Zhou, S., et al., 2016. Deep water drilling riser mechanical behavior analysis considering actual riser string configuration[J]. J. Nat. Gas Sci. Eng. 33, 240–254.
Pearce JL, Sizer PS, Gano JC, Yonker JH, Thurman RL, O'Sullivan JF, et al., 1988. Method and system for maintenance and servicing of subsea wells. United States Parent No. 4,730,677.
Santillan, S.T., Virgin, L.N., 2011. Numerical and experimental analysis of the static behavior of highly deformed risers[J]. Ocean Eng. 38 (13), 1397–1402.
Tian, Y., Hou, Y., Pires, F., et al., 2015. Tensioned Step Riser Configuration for Ultra-deep Application[C], ASME 2015, International Conference on Ocean, Offshore and Arctic Engineering. OMAE2015. V05AT04A056.
Wang, J., Duan, M., 2015. A nonlinear model for deepwater steel lazy-wave riser configuration with ocean current and internal flow[J]. Ocean Eng. 94, 155–162.
Wang, G., Liu, S.J., Li, L., 2007. FEM modeling for 3D dynamic analysis of deep-ocean mining pipeline and its experimental verification[J]. J. Cent. S. Univ. 14 (6), 808–813.
Yin, D., Passano, E., Lie, H., et al., 2019. Experimental and numerical study of a top tensioned riser subjected to vessel motion[J]. Ocean Eng. 171, 565–574.
Zienkiewicz, O.C., Taylor, R.L., 2005. The Finite Element Method[M].